

Mapping of the unoccupied states and relevant bosonic modes via the time dependent momentum distribution

A. F. Kemper,^{1,2,*} M. Sentef,² B. Moritz,^{3,2,4} C. C. Kao,⁵ Z. X. Shen,^{2,6} J. K. Freericks,⁷ and T. P. Devereaux^{2,6}

¹*Computational Research Division, Lawrence Berkeley National Laboratory, Berkeley, CA 94720, USA*

²*Stanford Institute for Materials and Energy Sciences,*

SLAC National Accelerator Laboratory, Menlo Park, CA 94025, USA

³*Department of Physics, Northern Illinois University, DeKalb, IL 60115, USA*

⁴*Department of Physics and Astrophysics, University of North Dakota, Grand Forks, ND 58202, USA*

⁵*Stanford Synchrotron Radiation Lightsource, SLAC National Accelerator Laboratory, Menlo Park, California 94025, USA*

⁶*Geballe Laboratory for Advanced Materials, Stanford University, Stanford, California 94305, USA*

⁷*Department of Physics, Georgetown University, Washington, DC 20057, USA*

The unoccupied states of complex materials are difficult to measure, yet play a key role in determining their properties. We propose a technique that can measure the unoccupied states, called time-resolved Compton scattering, which measures the time-dependent momentum distribution (TDMD). Using a non-equilibrium Keldysh formalism, we study the TDMD for electrons coupled to a lattice in a pump-probe setup. We find a direct relation between temporal oscillations in the TDMD and the dispersion of the underlying unoccupied states, suggesting that both can be measured by time-resolved Compton scattering. We demonstrate the experimental feasibility by applying the method to a model of MgB₂ with realistic material parameters.

PACS numbers: 78.47.je, 79.60.-i, 63.20.kd

I. INTRODUCTION

In understanding the emergent properties of complex materials, it is insufficient to limit ones' study solely to the occupied electronic states. The unoccupied states play an important role in determining, for example, the nature of the gap in charge- and spin-density waves, the absorption properties of semiconductors, or the magnetic properties of Mott systems. For example, without knowledge of the unoccupied states, it is difficult to measure both the size as well as the ordering wave vector \vec{q} of a gap in the electronic spectrum. Unfortunately, the most direct experimental measurements of momentum-resolved states in quantum materials, angle-resolved photoemission spectroscopy (ARPES), only determines the occupied states. This leaves the alternative methods of inverse photoemission spectroscopy, which lacks the signal strength to measure with sufficient resolution, or indirectly inferring the unoccupied dispersion from two-particle quantities such as optical spectroscopy. Pump-probe spectroscopy, and in particular time-resolved (tr-) ARPES, can measure part of the unoccupied states, but is limited by the inherent competition between temporal and energy resolution.

Here we consider a different quantity, where one sacrifices the energy information in favor of high time resolution, while maintaining high momentum resolution. We propose to measure the (gauge-invariant) time-dependent momentum distribution (TDMD) of quasiparticles, defined by $\langle c_{\mathbf{k}}^\dagger(t)c_{\mathbf{k}}(t) \rangle \equiv n_{\mathbf{k}}(t)$, which is similar to the so-called Wigner distribution.¹ It contains a rich amount of information about the behavior of pumped quasiparticles while avoiding some of the resolution-related complications of other measurements.

The TDMD is commonly measured via time-of-flight

absorption images in cold atomic gases, where it was recently used to map out the Fermi surface of a gas of ⁴⁰K atoms.² In the context of condensed matter systems, we propose two new types of measurements to access the TDMD. First, we propose to extend the technique of Compton scattering for solids into the time domain³. Compton scattering has a long history as a probe of the electron momentum distribution for solids in equilibrium⁴⁻⁶. With the advent of x-ray free-electron laser sources, the photon energy of the ultrashort x-ray probe pulses has been extended into the hard x-ray regime, where the fractional Compton cross-section becomes appreciable. With the advent of a hard x-ray free electron laser at the Linac Coherent Light Source, the photon energy will extend the energy of the x-ray free electron laser to beyond 20 keV. There is also significant progress in crystal optics at these energies, such that time-resolved high resolution Compton scattering with momentum resolution of a few percent of the Brillouin zone will be feasible. Additionally, recent developments in photonics suggest the future availability of ultrashort pulses ranging from x-rays to gamma rays⁷. Time-resolved Compton scattering has the advantage of using high-momentum photons, which can readily access the Brillouin zone edges in all directions. Secondly, one can access the TDMD with tr-ARPES by using similar time delays and probe pulse widths and integrating the tr-ARPES signal over energy (assuming the tr-ARPES signal comes from a single band near the Fermi level).

We illustrate the use of the TDMD by demonstrating how it can be used to map out the unoccupied dispersion in a pump-probe setup on a model system with electron-lattice interactions appropriate to a large class of complex materials. The TDMD exhibits two ubiquitous phenomena —both due to electron-phonon interac-

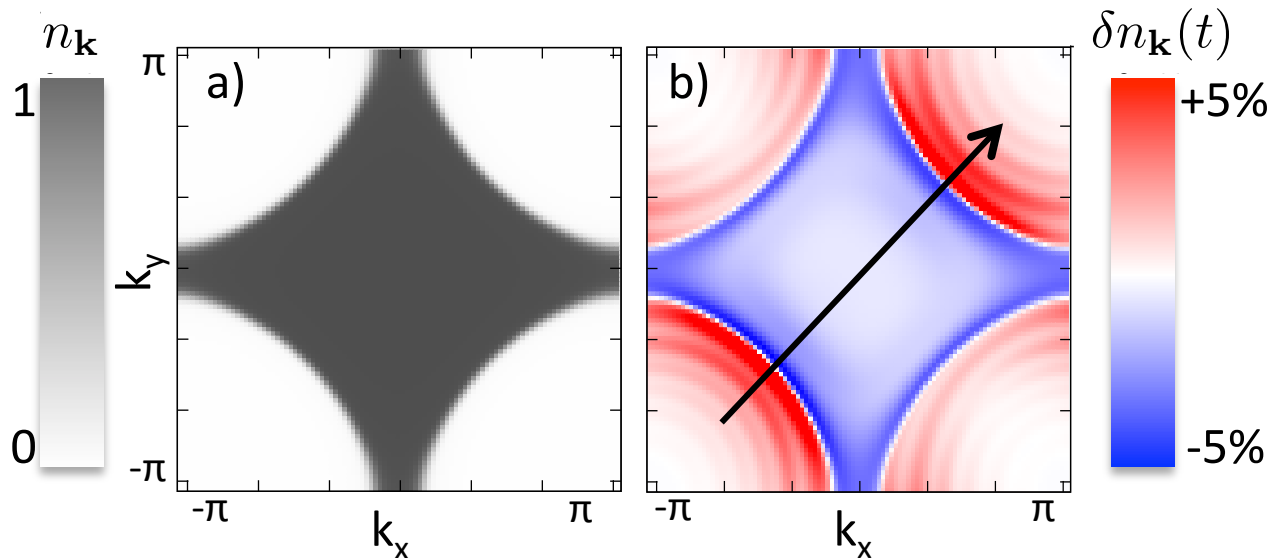


FIG. 1. a) (Color online) Equilibrium TDMD $n_{\mathbf{k}}(t)$ far before the pump arrives. The gray area indicates where quasiparticle states are occupied. The Fermi surface is sharply defined for the parameters presented ($g^2 = \sqrt{0.02V_{nn}}$, $T = 0.04V_{nn}$, $\Omega = 0.4V_{nn}$). b) Change in the momentum distribution from equilibrium $\delta n_{\mathbf{k}}(t)$ after a pump at $t \approx 4.8\tau_p$. The arrow indicates the direction of the applied electric field.

tions. First, the phonons dissipate the energy delivered to the electronic system by the pump. Second, after pumping, oscillations related to the phonon frequencies (and independent of the initial pump parameters) are commonly observed in the resulting spectra measured by the probe.^{8–11} We will show that both of these features are clearly seen in the TDMD, and that the oscillation frequencies can be analyzed to extract the underlying dispersion, in particular for the unoccupied states. Finally, we will demonstrate the feasibility of this technique by studying a model band structure for MgB_2 .

The paper shall proceed as follows. In Sec. II, we outline our method for calculations of two-time Green's functions on the Keldysh contour. In Sec. III, we present our results for the TDMD of a model system, and in Sec. IV, we apply the technique to the case of MgB_2 to demonstrate realistic capabilities of our method to map unoccupied states and their coupling to phonon spectra. A summary is presented in Sec. V.

II. METHOD

We study a two-dimensional system of electrons coupled to a bath of non-dispersive phonons with frequency Ω via a constant coupling g (known as the Holstein

model),¹².

$$\mathcal{H} = \sum_{\mathbf{k}\sigma} (\epsilon(\mathbf{k}) - \mu) c_{\mathbf{k},\sigma}^\dagger c_{\mathbf{k},\sigma} + \sum_{\mathbf{q}} \Omega b_{\mathbf{q}}^\dagger b_{\mathbf{q}} + g \sum_{\mathbf{k}\mathbf{q}\sigma} c_{\mathbf{k}+\mathbf{q},\sigma}^\dagger c_{\mathbf{k},\sigma} (b_{\mathbf{q}} + b_{-\mathbf{q}}^\dagger) \quad (1)$$

where $c_{\mathbf{k}}$ ($b_{\mathbf{q}}$) annihilates an electron (phonon) of momentum \mathbf{k} (\mathbf{q}).

While the TDMD is useful independent of the underlying model, here we use a band structure motivated by the transition-metal oxides: a 2D tight-binding $\epsilon(\mathbf{k})$ with (next) nearest-neighbor hoppings V_{nn} and $V_{nnn} = 0.3V_{nn}$, and $\mu = -1.02V_{nn}$. We use the conventions $\hbar = e = c = 1$. Below, we will report timescales in units of a characteristic phonon timescale $\tau_p = 1/\Omega$. For example, a phonon with an energy of $\Omega = 10$ meV has $\tau_p \approx 0.4$ ps. Similarly, there is a characteristic electron timescale $\tau_e = 1/V_{nn} \approx 16$ fs for $V_{nn} = 250$ meV. Although in this work we will explicitly examine higher energy phonons for numerical stability reasons, the results below occur due to the relevant energy scales in the problem, and will simply be rescaled to lower phonon energies.

To describe the non-equilibrium pump-probe process, we propagate the system on the Kadanoff-Baym-Keldysh (Keldysh) contour¹³, which has been described in detail elsewhere^{1,14,15}. The non-equilibrium Keldysh formalism has been successfully used to describe the time evolution of correlated electrons within dynamical mean-field theory^{16–19}. The electric field is included through the standard Peierls' substitution $\mathbf{k} \rightarrow \mathbf{k} - \mathbf{A}(t)$, where the

vector potential \mathbf{A} is related to the applied electric field \mathbf{F} via $-\partial\mathbf{A}(t)/\partial t = \mathbf{F}$ and we work in the Hamiltonian gauge.

Within the Migdal limit, we consider the renormalization of the electron Green's function by a single phonon emission/absorption and ignore the phonon self-energy (as is done in conventional Migdal-Eliashberg theory). In this limit, we solve the Dyson equation

$$G_{\mathbf{k}}(t, t') = G_{\mathbf{k}}^0(t, t') + \int_c dt_1 dt_2 G_{\mathbf{k}}^0(t, t_1) \Sigma(t_1, t_2) G_{\mathbf{k}}(t_2, t')$$

with the self-energy $\Sigma(t, t') = ig^2 \sum_{\mathbf{k}} D^0(t, t') G_{\mathbf{k}}^0(t, t')$, where $G_{\mathbf{k}}^0(t, t')$ and $D^0(t, t')$ are the non-interacting electron and phonon Green's functions, respectively¹. The Dyson equation can be solved by recasting it as a matrix equation¹⁵ or by decomposing into Volterra-type equations through the Langreth rules²⁰, which is the approach used here.

III. RESULTS

Figure 1 shows the gauge-invariant TDMD $n_{\mathbf{k}}(t) = iG_{\mathbf{k}+\vec{A}(t)}^<(t, t' \rightarrow t)$ for $g = \sqrt{0.02}V_{nn}$, $\Omega = 0.4V_{nn}$ and at an initial temperature $T = 0.04V_{nn}$. Fig. 1 (a) shows $n_{\mathbf{k}}(t)$ at times far before the pump, where the system is fully described by the equilibrium problem. To clearly show the changes for the small pump fluences considered ($F_{max} \leq 4V_{nn}$), Fig. 1 (b) shows the change in the TDMD from equilibrium: $\delta n_{\mathbf{k}}(t) \equiv n_{\mathbf{k}}(t) - n_{\mathbf{k}}(t \rightarrow -\infty)$.

We apply a pulse centered at time $t = 0$ in the (11) (diagonal) direction of the form $A(t) = (F_{max}/\omega_A) \exp(-t^2/(2\sigma^2)) \sin(\omega_A t)$, with a maximum field strength of $F_{max} = 4V_{nn}$, a frequency $\omega_A = 2V_{nn}$ and $\sigma \approx 0.4\tau_p$. At the time shown in Fig. 1 (b), the pump has passed, and the system is relaxing towards equilibrium. The C_4 symmetry of $n_{\mathbf{k}}(t)$ in equilibrium is broken by the field (which points in the (11) direction as shown by the black arrow), and this is reflected in the transient change. In fact, this can be used to emphasize particular regions of interest in the Brillouin zone. By rotating the field, the regions exhibiting the largest change in $n_{\mathbf{k}}(t)$ will shift with the field direction, providing access to new regions by emphasizing the experimental signal near different momenta.

First, we consider the anisotropic redistribution of quasiparticles as a function of time. In Figure 2 (a), we show $\delta n_{\mathbf{k}}(t)$ at the momenta indicated in the inset; the blue (black) momenta have the same energy $\epsilon_{\mathbf{k}}$ but due to the C_4 symmetry breaking have different time traces (Fig. 2 (b)). From the figure, one can clearly see that there is a difference in the overall magnitude of the change at the equivalent momenta (with the same color). The solid lines are fits to the amplitude of a simple decaying exponential, where we have taken the decay constant at a momentum \mathbf{k} from the on-shell equilibrium self-energy $1/\tau_{\mathbf{k}}(\omega) = -2\text{Im} \Sigma(\omega = \epsilon_{\mathbf{k}})$ shown in Fig. 2

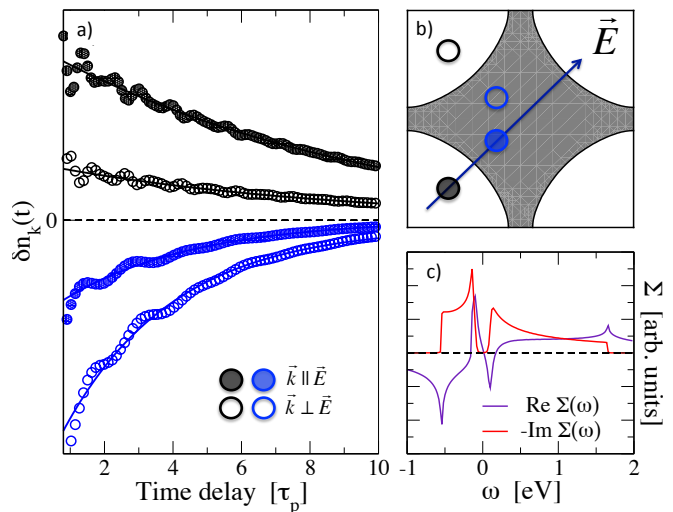


FIG. 2. a) (Color online) Change in the TDMD $n_{\mathbf{k}}(t)$ from the equilibrium value (at $t = 0$) for the points in the Brillouin zone indicated in b). Symbols are calculated data points (for clarity, not all are shown), solid lines are fits to an exponential decay using a fixed relaxation rate $1/\tau_{\mathbf{k}} = -2\text{Im} \Sigma(\omega = \epsilon_{\mathbf{k}})$. c) Real and imaginary parts of the equilibrium self-energy $\Sigma(\omega)$ for the parameters in a) ($g = \sqrt{0.02}V_{nn}$, $T = 0.04V_{nn}$, $\Omega = 0.4V_{nn}$).

(c), as suggested by a recent study²¹. The remarkable agreement with the calculated data points confirms that it is indeed the equilibrium self-energy that controls the decay rate. Since the equilibrium self-energy is C_4 symmetric, the anisotropic redistribution in $\delta n_{\mathbf{k}}(t)$ is caused by the C_4 symmetry breaking of the applied pump field.

On top of the decay are oscillations dominated by a few characteristic frequencies, as often observed in pump-probe experiments.⁸⁻¹¹ These are clearly observed as rings in $\delta n_{\mathbf{k}}(t)$ shown in Fig. 1, as well as oscillations in the time traces in Fig. 2 (a). We further emphasize these in Fig. 3, where we have subtracted the decaying exponential from several points along the Brillouin zone diagonal in Fig. 1. From Fig. 3 (a), one can observe two main features. First, the oscillation frequencies in the time traces depend strongly on momentum. Second, although there is only a single phonon frequency in our model, several oscillation frequencies can be observed. Figure 3 (b) shows the Fourier transform power spectrum of the oscillations in Fig. 3 (a). Each curve has readily visible maxima, in addition to some smaller structure across the frequency spectrum. For each energy (momentum) $\epsilon_{\mathbf{k}}$, the vertical lines indicate the energies $\omega = \epsilon_{\mathbf{k}} + \Omega$ and $\omega = \epsilon_{\mathbf{k}} - W_- + \Omega$, where W_- is the energy at the bottom of the band (at $\mathbf{k} = \Gamma$).

The temporal dynamics of the Holstein model leads to this rich physics. The decay and the oscillations observed are momentum (energy) dependent, and their amplitudes depend on the electron-phonon coupling, as well as the applied field. Describing the full temporal dynamics of $n_{\mathbf{k}}(t)$ is complicated, yet we can gain some insight by

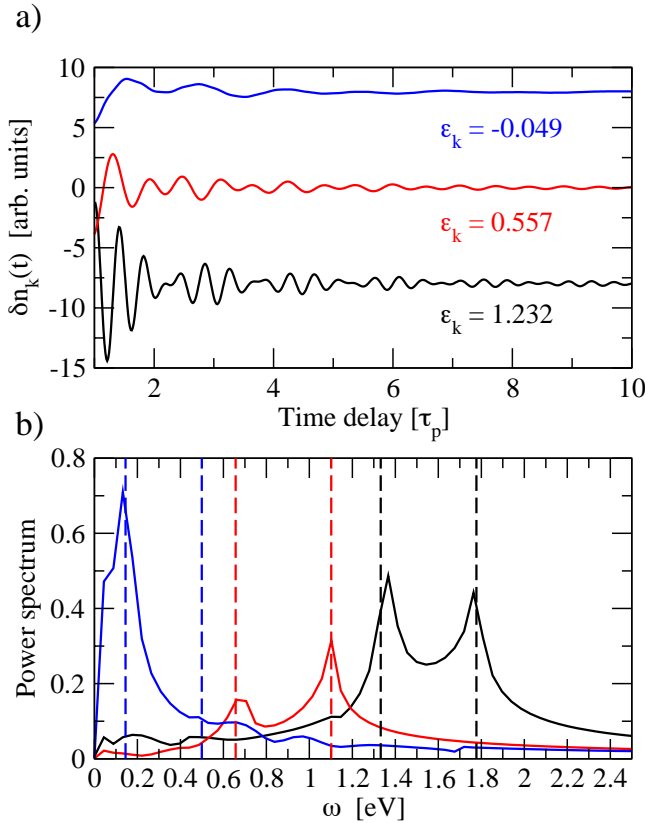


FIG. 3. a) (Color online) Oscillatory part of $\delta n_{\mathbf{k}}(t)$ for \mathbf{k} along (11) at the energies $\epsilon_{\mathbf{k}}$ indicated (offset for clarity). b) Fourier transform of a). Vertical lines indicate the frequencies corresponding to the strong oscillations on the unoccupied side, $\omega = \epsilon_{\mathbf{k}} + \Omega$ and $\omega = \epsilon_{\mathbf{k}} - W_- + \Omega$. In both a) and b) the oscillations on the unoccupied side close to the Fermi level (blue curves) have been scaled down by 4 for visibility. (see text for details).

focusing on the times where the pump is off, while the system is still displaced from its equilibrium configuration. The subsequent relaxation occurs from the new configuration through the equations of motion. In equilibrium, the TDMD is balanced by equal rates of in- and out-scattering; once the pump breaks this symmetry, the system relaxes back to the equilibrium according to the dynamics contained within the self-energy and Green's functions. In addition to the relaxation, the TDMD oscillates at the band energy shifted by the characteristic energies in the problem (the phonon frequency and bandwidth) at which the self-energy is largest. This is shown analytically at $T = 0$ in the appendix; the full calculation requires the numerical methods used here.

At low temperatures, the real part of the self-energy Σ' is large and peaked near four frequencies, $\omega = \pm\Omega$ and $\omega = W_{\pm} \pm \Omega$, where W_{\pm} is the upper (lower) band edge (see Fig. 3(b)). The resulting $n_{\mathbf{k}}(t)$ oscillates at the band energy $\epsilon_{\mathbf{k}}$ shifted by those frequencies. In principle, all four frequencies should be observable in the power spec-

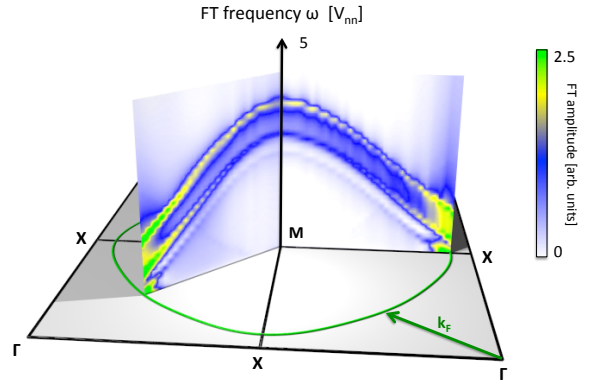


FIG. 4. (Color online) Fourier power spectrum of the oscillation frequencies along the Γ -M and M-X directions in the unoccupied Brillouin zone. The two strong peaks in the Fourier spectra follow the lines corresponding to phonon emission processes; a small tertiary line of peaks can be seen at lower frequencies corresponding to a phonon absorption process. The Fermi surface is shown in green on the base plane.

trum of Fig. 3; however, two frequencies (with the positive sign above) correspond to phonon absorption, which is small at low temperatures, and thus the corresponding peaks in the power spectrum are reduced significantly. The two strong peaks expected for the unoccupied side are indicated in Fig. 3 by vertical lines, which agree well with the observed frequencies, up to a small shift in energy due to $\Sigma'(\omega = 0)$ which is normally absorbed into the chemical potential μ . An interesting consequence of the expected oscillation frequencies is that if one considers a measurement near the Fermi level, the oscillations will appear to be strongest at just the phonon frequency (as in recent tr-ARPES experiments⁸⁻¹¹).

The simple dependence of the oscillation frequencies on the underlying band structure suggests a novel method to measure the electron dispersion by looking at the oscillations in the TDMD. The oscillations are most clearly visible in the unoccupied region of the Brillouin zone, which is exactly the region that traditional methods for measuring the dispersion have difficulty accessing. By tracking the oscillation frequencies as a function of momentum one can directly map out the dispersion. In Fig. 4, we plot the Fourier transform power spectrum in the unoccupied portion of the Brillouin zone along the zone diagonal and zone face. This shows most clearly the two strong peaks in the Fourier transform associated with phonon emission, although a weaker line corresponding to phonon absorption is also visible below the two main lines. All three lines, up to the constant shifts from $\Sigma'(0)$, W_{\pm} and Ω , follow the unoccupied dispersion. Thus, from the maxima in the power spectrum the unoccupied dispersion can be directly measured.

The high temporal resolution afforded by the neglect of any frequency information (in contrast with tr-ARPES) allows these oscillations to be clearly resolved. Furthermore, the oscillations are strongest in the direction of the

applied field. This gives the method an additional degree of freedom, where the field direction can be used to select the momentum cuts of interest. Measuring the TDMD thus provides complementary information to that gained from other time-resolved experiments. Additionally, we have shown that there is a direct connection between the oscillations in the TDMD and $\Sigma'(\omega)$. This is the complement to the recent work by Sentef et al.²¹, where it was shown that the *imaginary* part of the self-energy $\Sigma''(\omega)$ can be inferred from decay rates in tr-ARPES.

IV. A CASE STUDY: MgB₂

The above analysis, applied to theoretical results, can be applied to experimental results equally well. Here, the experimental capabilities must be considered. The salient points to consider are as follows. First, the experimental time resolution will place an upper bound on the oscillation frequencies that can be resolved. This will limit the measurement capability to regions near the Fermi level; fortunately, this is generally where one wishes to measure, and thus the experimental resolution only limits the upper bound of resolvability. Second, materials have more than a single Holstein phonon mode, which should be taken into account. In this section, we repeat the calculations done previously, but for a band structure appropriate to MgB₂.²² Furthermore, we couple the electronic system to a distribution of phonons through a model $\alpha^2F(\omega)$, which we have constructed based on experimentally broadened phonon frequencies calculated from first-principles.²³

Fig. 5 shows the model $\alpha^2F(\omega)$ used in the calculations. For calculations of the TDMD, we focus on the π bonding band of MgB₂, along the line $k_y = 0, k_z = 0$ of the band structure

$$\epsilon_\pi(\mathbf{k}) = e_\pi + 2t_\perp \cos k_z - t'_\parallel \sqrt{1 + 4 \cos \frac{k_y}{2} \left(\cos \frac{k_y}{2} + \cos \frac{k_x \sqrt{3}}{2} \right)}, \quad (2)$$

where $e_\pi = 0.04$ eV, $t_\perp = 0.92$ eV, and $t'_\parallel = 1.60$ eV, and the Fermi level is set to 0.²²

In principle, the redistribution of quasiparticles during the pump in a multi-band system is complex; however, here we focus entirely on the decay of the excitations after the pump, which are determined by the equilibrium, intra-band self-energy. Furthermore, our intent here is to include realistic material properties to show that this signal can, in fact, be measured. As such, we perform the calculations for the π bonding band only. Since the self-energy is a priori unknown (unlike in the model calculation), we have fitted an exponential to the time traces. The fitted exponential is subtracted from the time traces, which are subsequently Fourier transformed. The Fourier transform power spectrum is shown as a false-color intensity map for a cut along the zone

boundary in Fig. 5. The red lines on the plot indicate the expected oscillation frequencies for a single mode at $\Omega = 65$ meV, namely (the larger) $\omega_1 = |\epsilon(\mathbf{k}) + \Omega|$ and (near the Fermi level) $\omega_2 = |\epsilon(\mathbf{k}) + \Omega + W|$, where W is the top of the band. Although a full phonon distribution is included through $\alpha^2F(\omega)$, the presence of a strongly coupled mode allows for the resolution of a single dispersive mode, although broadened. The agreement with the predicted frequencies and the observed ones indicates that our previous conclusions hold, even in the presence of multiple phonon modes. The observation that the power spectrum is dominated by the single broadened mode for a realistic phonon spectrum justifies the use of a single Holstein mode previously, as it captures the essential features seen here. The final, orange dashed line on the plot indicates the experimental resolution bound for a probe resolution of 10 fs.

The further experimental considerations involve scattering matrix elements, and the distinction between real and crystal momentum. These issues have been discussed in some detail (in equilibrium) previously, and the arguments presented there hold in non-equilibrium as well.^{4,24}

V. SUMMARY

We have shown the use of the time-dependent momentum distribution as a novel concept in the understanding of time-resolved spectroscopy, and non-equilibrium phenomena in general. The decay rates and the oscillations in the time traces of the TDMD were shown to be directly related to the underlying equilibrium self-energy. This result is of importance in time-resolved spectroscopy, where it has long been assumed that the equilibrium properties can be studied in a time-resolved experiment. We further have shown that the TDMD can be directly measured by an experiment that only has momentum and time resolution, such as time-resolved Compton scattering and energy-integrated time-resolved ARPES. Experimentally, the width of the probe pulse limits the temporal resolution of the TDMD. However, in many systems of interest, the features one wishes to investigate lie near the Fermi level, both above and below. For example, in the high-T_c cuprates, several features are predicted to lie within this energy range.²⁵ In other gapped systems, without the knowledge of the spectra above the Fermi level it is impossible to correctly assign the gap magnitude. Similar effects due to spin fluctuations, phonons, and other interesting collective and bosonic features lie at low energy, and are thus accessible by this technique.

ACKNOWLEDGMENTS

Acknowledgments AFK, MS, BM and TPD were supported by the U.S. Department of Energy, Basic En-

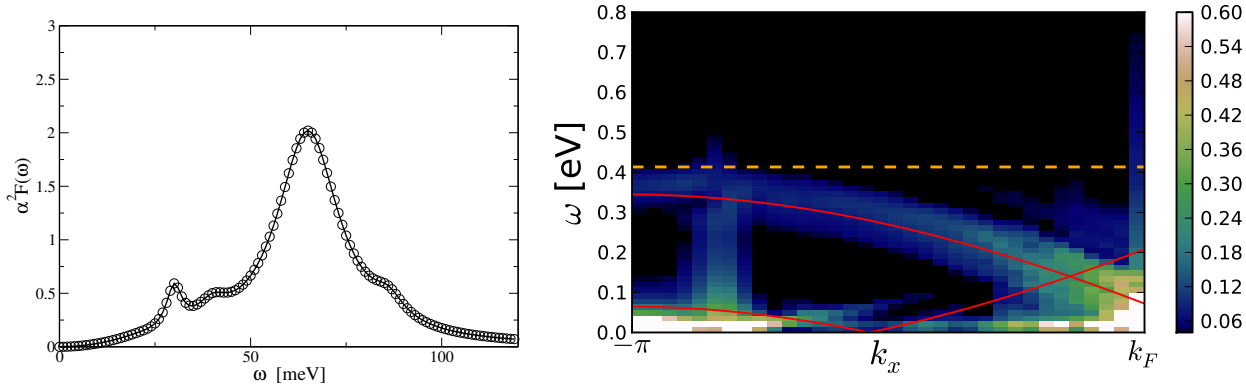


FIG. 5. (Color online) Left: Model $\alpha^2 F(\omega)$ for MgB₂ used in the calculations. Right: Fourier power spectrum of the oscillation frequencies near the π bonding band in MgB₂. The red lines indicate the expected frequencies due to emission of a phonon of 65 meV, and the orange line indicates an resolution upper bound for a temporal resolution of 10 fs.

ergy Sciences, Materials Sciences and Engineering Division under contract No. DE-AC02-76SF00515. JKF was supported by the U.S. Department of Energy, Basic Energy Sciences, Materials Sciences and Engineering Division under contract No. DE-FG02-08ER46542 and by the McDevitt bequest at Georgetown University. The collaboration was supported by the U.S. Department of Energy, Basic Energy Sciences, Materials Sciences and Engineering Division under contract Nos. DE-FG02-08ER46540 and DE-SC0007091. This work was made possible by the resources of the National Energy Research Scientific Computing Center which is supported by the U.S.

DOE, Office of Science, under Contract No. DE-AC02-05CH11231. We gratefully acknowledge discussions with P. S. Kirchmann, J. Sobota, M. Wolf, and S. Yang.

Appendix: Analytic calculation of oscillations

We can explain the oscillations in the TDMD by examining the equations of motion for the mixed and lesser Green's functions at $T = 0$ (where the state is fully described without a thermal average). Following the Langreth rules, we obtain the following Volterra-type equations²⁰,

$$[i\partial_t - h(t)] G_{\mathbf{p}}^{ri}(t, 0) = \int_0^t d\bar{t} \Sigma^R(t, \bar{t}) G_{\mathbf{p}}^{ri}(\bar{t}, 0) \quad (\text{A.1})$$

$$G_{\mathbf{p}}^{ri}(0, 0) = i n_{\mathbf{p}}$$

$$[i\partial_t - h(t)] G_{\mathbf{p}}^{<}(t, t') = \int_0^t d\bar{t} \Sigma^R(t, \bar{t}) G_{\mathbf{p}}^{<}(\bar{t}, t') + \int_0^{t'} d\bar{t} \Sigma^{<}(t, \bar{t}) G_{\mathbf{p}}^A(\bar{t}, t') \quad (\text{A.2})$$

$$G_{\mathbf{p}}^{<}(0, t') = -G_{\mathbf{p}}^{ri}(t', 0)^*$$

where $h(t) = \epsilon(\mathbf{k} - \mathbf{A}(t))$, $\epsilon(\mathbf{k})$ is the dispersion, and $n_{\mathbf{p}}$ is the Fermi function at energy $\epsilon_{\mathbf{p}}$. The superscripts $<$ and ri denote the “lesser” and mixed components of the Green's function and self-energy, respectively.

In the absence of a driving field or interactions, we obtain the known results for the mixed and lesser Green's functions

$$G_{0\mathbf{p}}^{ri}(t, 0) = i n_{\mathbf{p}} e^{-i\epsilon_{\mathbf{p}} t}$$

$$G_{0\mathbf{p}}^{<}(t, t') = i n_{\mathbf{p}} e^{-i\epsilon_{\mathbf{p}}(t-t')}$$

We are interested in the oscillations of the TDMD after the pump is off, when the system is out of its equilibrium state. Since we are interested in the dynamics, in lieu of driving the system explicitly with a field, we turn on the interactions at an infinitesimal time after zero ($t = 0^+$). By construction, this problem has the same dynamics as those of the relaxation after driving by a pump. This, coupled with the approximation of weak interactions (where we replace the full Green's function on the right hand side with the bare one), allows us to obtain analytic formulae which show the oscillation dynamics. We shall consider the change of the equilibrium

Green's functions $\Delta G = G - G_0$. First, we solve equation of motion for $\Delta G^{ri}(t)$, which we shall need as an initial condition for the TDMD. $\Delta G^{ri}(t)$ has no initial condition

beyond that for the bare Green's function $G_0^{ri}(t)$.

$$\Delta G_{\mathbf{p}}^{ri}(t, 0) = ig^2 n_{\mathbf{p}} \sum_{\mathbf{k}} \left[\frac{n_{\mathbf{k}}}{(\epsilon_{\mathbf{k}} - \Omega - \epsilon_{\mathbf{p}})^2} F(-\Omega) + \frac{1 - n_{\mathbf{k}}}{(\epsilon_{\mathbf{k}} + \Omega - \epsilon_{\mathbf{p}})^2} F(\Omega) \right] \quad (\text{A.3})$$

$$F(\Omega) = e^{-i(\epsilon_{\mathbf{k}} + \Omega)t} + e^{-i\epsilon_{\mathbf{p}}t} [i(\epsilon_{\mathbf{k}} + \Omega - \epsilon_{\mathbf{p}})t - 1]$$

We proceed by similarly solving the equation for the lesser component. The full expressions are complex, but can be significantly simplified by considering the case where $t' \rightarrow t$,

$$\begin{aligned} \Delta G_{\mathbf{p}}^<(t, t') &= -G^{ri}(t)^* e^{-i\epsilon_{\mathbf{p}}t} + ig^2 n_{\mathbf{p}} \sum_{\mathbf{k}} \left[\frac{n_{\mathbf{k}}}{(\epsilon_{\mathbf{k}} - \Omega - \epsilon_{\mathbf{p}})^2} F(-\Omega) + \frac{1 - n_{\mathbf{k}}}{(\epsilon_{\mathbf{k}} + \Omega - \epsilon_{\mathbf{p}})^2} F(\Omega) - \frac{2 \cos[(\epsilon_{\mathbf{k}} - \Omega - \epsilon_{\mathbf{p}})t] - 2}{(\epsilon_{\mathbf{k}} - \Omega + \epsilon_{\mathbf{p}})^2} \right] \\ &= 2ig^2 n_{\mathbf{p}} \sum_{\mathbf{k}} (1 - n_{\mathbf{k}}) \left[\frac{\cos[(\epsilon_{\mathbf{k}} + \Omega - \epsilon_{\mathbf{p}})t] - 1}{(\epsilon_{\mathbf{k}} + \Omega - \epsilon_{\mathbf{p}})^2} - \frac{\cos[(\epsilon_{\mathbf{k}} - \Omega - \epsilon_{\mathbf{p}})t] - 1}{(\epsilon_{\mathbf{k}} - \Omega - \epsilon_{\mathbf{p}})^2} \right] \end{aligned} \quad (\text{A.4})$$

Now, only the integral over the \mathbf{k} states remains. We shall assume that the density of states is flat over the region we integrate over (and equal to N_0), and has band edges at $\pm W$. This results in integrals of the form

$$\int_0^W dx \frac{\cos[(x \pm \Omega - \epsilon_{\mathbf{p}})t] - 1}{(x \pm \Omega - \epsilon_{\mathbf{p}})^2} = \frac{\cos[(x \pm \Omega - \epsilon_{\mathbf{p}})t] - 1}{x \pm \Omega - \epsilon_{\mathbf{p}}} - t\mathcal{S}[(x \pm \Omega - \epsilon_{\mathbf{p}})t] \Big|_0^W \quad (\text{A.5})$$

Here, \mathcal{S} denotes the sine integral. Thus, the two terms each show two distinct oscillation frequencies, $\omega = \epsilon_{\mathbf{p}} \pm \Omega$

and $\omega = \epsilon_{\mathbf{p}} \pm (\Omega + W)$. Figure 6 shows the change in the TDMD as the interactions are turned on in an infinite band. Here, the oscillations occur at $\epsilon_{\mathbf{p}} \pm \Omega$, although those where $|\epsilon_{\mathbf{p}} - \Omega|$ is smallest dominate the signal.

In the course of this calculation, a number of approximations were made. Nevertheless, the oscillation frequencies agree with those observed from the full numerical simulations. The inclusion of the correct density of states, as well as the replacement of the bare Green's functions will cause a small shift of the frequencies observed, and a distribution of frequencies centered around the bare one shown here.

* afkemper@lbl.gov

¹ For a complete description of the non-interacting Green's functions see e.g. G. Mahan, *Many-Particle Physics* (Plenum Press, NY, 1990).

² T. E. Drake, Y. Sagi, R. Paudel, J. T. Stewart, J. P. Gaebler, and D. S. Jin, *Phys. Rev. A* **86**, 031601 (2012).

³ Time-resolved Compton scattering in 1D was previously studied by R. E. Wagner, Q. Su, and R. Grobe, *Phys. Rev. A* **82**, 022719 (2010).

⁴ M. J. Cooper, *Reports on Progress in Physics* **48**, 415 (1985).

⁵ A. Bansil, B. Barbiellini, S. Kaprzyk, and P. Mijnaerends, *J. Phys. Chem. of Solids* **62**, 2191 (2001).

⁶ Y. Sakurai, M. Itou, B. Barbiellini, P. E. Mijnaerends, R. S. Markiewicz, S. Kaprzyk, J. M. Gillet, S. Wakimoto, M. Fujita, S. Basak, Y. J. Wang, W. Al-Sawai, H. Lin, A. Bansil,

and K. Yamada, *Science* **332**, 698 (2011).

⁷ K. Ta Phuoc, S. Corde, C. Thauray, V. Malka, A. Tafzi, J. P. Goddet, R. C. Shah, S. Sebban, and A. Rousse, *Nature Photonics* **6**, 308 (2012).

⁸ F. Schmitt, P. S. Kirchmann, U. Bovensiepen, R. G. Moore, L. Rettig, M. Krenz, J. H. Chu, N. Ru, L. Perfetti, D. H. Lu, M. Wolf, I. R. Fisher, and Z. X. Shen, *Science* **321**, 1649 (2008).

⁹ L. Perfetti, P. A. Loukakos, M. Lisowski, U. Bovensiepen, M. Wolf, H. Berger, S. Biermann, and A. Georges, *New. J. Phys.* **10**, 053019 (2008).

¹⁰ L. Rettig, R. Cortés, S. Thirupathaiah, P. Gegenwart, H. S. Jeevan, T. Wolf, U. Bovensiepen, M. Wolf, H. A. Dürr, and J. Fink, preprint (2010), arXiv:1008.1561.

¹¹ K. W. Kim, A. Pashkin, H. Schäfer, M. Beyer, M. Porer, T. Wolf, C. Bernhard, J. Demsar, R. Huber, and A. Leit-

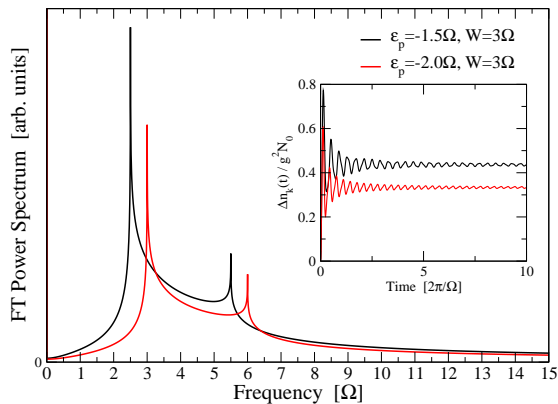


FIG. 6. Change in the TDMD after turning on interactions for an infinite band.

enstorfer, *Nature Materials* (2012).

- ¹² T. Holstein, *Ann. Phys.* **8**, 325 (1959); **8**, 343 (1959).
¹³ L. P. Kadanoff and G. Baym, *Quantum Statistical Mechanics* (W. A. Benjamin, Inc., NY, 1962); L. V. Keldysh, *Zh. Eksp. Teor. Fiz.* **47**, 1515 (1964).
¹⁴ A. P. Jauho and J. W. Wilkins, *Phys. Rev. B* **29**, 1919 (1984); J. H. Davies and J. W. Wilkins, *Phys. Rev. B* **38**,

- 1667 (1988).
¹⁵ V. Turkowski and J. K. Freericks, *Phys. Rev. B* **71**, 085104 (2005); J. K. Freericks, *Phys. Rev. B* **77**, 075109 (2008).
¹⁶ M. Eckstein and M. Kollar, *Phys. Rev. Lett.* **100**, 120404 (2008); M. Eckstein, A. Hackl, S. Kehrein, M. Kollar, M. Moeckel, P. Werner, and F. A. Wolf, *Eur. Phys. J.: S.T.* **180**, 217 (2009); M. Eckstein, M. Kollar, and P. Werner, *Phys. Rev. Lett.* **103**, 056403 (2009).
¹⁷ B. Moritz, T. P. Devereaux, and J. K. Freericks, *Phys. Rev. B* **81**, 165112 (2010).
¹⁸ M. Eckstein, M. Kollar, and P. Werner, *Phys. Rev. B* **81**, 115131 (2010).
¹⁹ B. Moritz, T. P. Devereaux, and J. K. Freericks, *Comp. Phys. Comm.* **182**, 109 (2011); B. Moritz, A. F. Kemper, M. Sentef, T. P. Devereaux, and J. K. Freericks, preprint (2012), arXiv:1207.3835.
²⁰ R. van Leeuwen, N. E. Dahlen, G. Stefanucci, C.-O. Almbladh, and U. von Barth, preprint (2005), arXiv:cond-mat/0506130.
²¹ M. Sentef, A. F. Kemper, B. Moritz, J. K. Freericks, Z.-X. Shen, and T. P. Devereaux, preprint (2012), arXiv:1212.4841.
²² K. Szalowski, *Phys. Rev. B* **74**, 094501 (2006).
²³ K.-P. Bohnen, R. Heid, and B. Renker, *Phys. Rev. Lett.* **86**, 5771 (2001).
²⁴ W. Schülke, G. Stutz, F. Wohlert, and A. Kaprolat, *Phys. Rev. B* **54**, 14381 (1996).
²⁵ B. Moritz, F. Schmitt, W. Meevasana, S. Johnston, E. M. Motoyama, M. Greven, D. H. Lu, C. Kim, R. T. Scalettar, Z.-X. Shen, and T. P. Devereaux, *New Journal of Physics* **11**, 093020 (2009).